

Mobility-Aware Resource Allocation for mmWave IAB Networks: A Multi-Agent RL Approach

Bibo Zhang and Ilario Filippini, *Senior Member, IEEE*

Abstract—MmWaves have been envisioned as a promising direction to provide Gbps wireless access. However, they are susceptible to high path losses and blockages, which directional antennas can only partially mitigate. That makes mmWave networks coverage-limited, thus requiring dense deployments. Integrated access and backhaul (IAB) architectures have emerged as a cost-effective solution for network densification. Resource allocation in mmWave IAB networks must face big challenges to cope with heavy temporal dynamics, such as intermittent links caused by user mobility and blockages from moving obstacles. This makes it extremely difficult to find optimal and adaptive solutions. In this article, exploiting the distributed structure of the problem, we propose a Multi-Agent Reinforcement Learning (MARL) framework to optimize user throughput via flow routing and link scheduling in mmWave IAB networks characterized by user mobility and link outages generated by moving obstacles. The proposed approach implicitly captures the environment dynamics, coordinates the interference, and manages the buffer levels of IAB relay nodes. We design different MARL components, considering full-duplex and half-duplex IAB-nodes. In addition, we provide a communication and coordination scheme for RL agents in an online training framework, addressing the feasibility issues of practical systems. Numerical results show the effectiveness of the proposed approach.

Index Terms—mmWave networks, integrated access and backhaul (IAB), resource allocation, user mobility, obstacle blockages, multi-agent reinforcement learning (MARL).



1 INTRODUCTION

THE availability of millimeter-wave (mmWave) bands for radio access networks (RANs) in the 5G standardization has been considered by the 3rd Generation Partnership Project (3GPP) as one of the main reliefs to the explosive increase of the global mobile traffic, which is now posing big challenges to the access capacity provided by sub-6GHz communications. The large bandwidths (several hundreds of MHz) and mainly-underutilized spectrum portions available at those high frequencies are the key enablers of a Gbps access throughput.

However, this potential comes at a cost of facing a harsh propagation environment characterized by very high path losses and no propagation through obstacles, including not only static buildings but also moving vehicles and pedestrians. While current antenna design technologies have shown to be effective in mitigating these path losses through extremely directional arrays, there is very little they can do against random blockages. In practice, mmWave networks typically exhibit a coverage-limited behavior due to the presence of obstacles. Therefore, to guarantee a high-quality coverage, 5G mmWave access networks require base stations to be much more densely deployed than in traditional radio access networks. This may translate into high installation budgets for operators, which are mainly driven by costs to deploy wired (e.g., fiber) backhaul connections.

Aiming to provide a dense network deployment at minimal costs, Release 16 of 3GPP specifications has introduced a new multi-hop wireless access architecture, named Integrated Access and Backhaul (IAB)[1]. The rationale is to

place relay nodes, called IAB-nodes, in the service area of a mmWave base station (BS), called IAB-donor, and form a wireless multi-hop backhaul to forward data packets between the IAB-donor and user equipments (UEs). An example of such an IAB network scenario can be found in Fig. 1. Self-backhauling is a peculiar aspect of this architecture, where both radio access and backhaul links share the same radio resources and interfaces. Therefore, a proper radio resource allocation is essential to efficiently operate this network. In particular, since the adopted multiple access scheme is based on time-division multiple access (TDMA), the resource optimization must deal with routing paths and scheduling of directional transmissions along established links.

Studies on routing and scheduling in wireless multi-hop networks have appeared in the literature since early 2000s, mainly resorting to optimization techniques that assume always-available links and static users [2, 3]. However, it is hard for these techniques to provide mobile mmWave IAB networks with practical solutions that simultaneously deal with the harsh propagation environment, the strong impact of obstacles on link availability, and the users' mobility. Indeed, the optimal solution provided under ideal link conditions typically underperforms when facing the stochastic on-off link behavior caused by sudden obstacles and the dynamics of mobile users, which can even eliminate all the advantages of a careful optimization. We could in principle re-optimize the network periodically or every time it undergoes a change, however, this will lead to huge computational costs and, most likely, it would not be practical. Therefore, flexible and adaptive solutions are required to schedule real-time operations so as to tackle random obstacles and users' mobility.

• Authors are with Dipartimento di Elettronica, Informazione e Bioingegneria, Politecnico di Milano, Milan, Italy, 20133. E-mail: name.surname@polimi.it

Given the above context, we believe that Reinforcement Learning (RL) techniques can play an important role due to their intrinsic ability to adapt to the behavior of the environment. Indeed, an RL agent can be trained by playing against the environment and eventually discover a good strategy, even when the environment’s reply is stochastic. RL agents can automatically grasp relevant environment statistics during the training and apply the strategy that provides the best long-term reward in front of any instance of the random environment. Moreover, routing and scheduling in wireless multi-hop networks have been traditionally considered as hard problems due to interference constraints. They become even harder when user mobility and random obstacles are introduced. Links’ availability is intermittent, which makes it impossible to harness traditional approaches that are based on sets of potential concurrent transmissions (i.e., compatible links) because the sets will change as users arbitrarily move around or links get randomly blocked.

Random mobility patterns characterizing both UEs and obstacles typically generate local areas with local statistics that may differ from the others across the network. To leverage such a diverse structure of the problem, Multi-Agent Reinforcement Learning (MARL) techniques can be used to exploit multiple RL agents able to both make decisions based on local observations and coordinate with other agents. This allows to split a single, complex, and high-dimensional problem – which would otherwise be intractable – into several, cooperative, and low-dimensional tasks.

In this article, we address the joint flow routing and link scheduling problem in mmWave IAB networks, coordinating both access and backhaul transmissions to maximize the downlink throughput perceived by UEs. We provide the first MARL framework for such networks, which is able to perform real-time operations, taking into account the IAB-nodes’ buffer levels to avoid multi-hop starvation, the stochastic behavior of mmWave communications to rely on the best links, and the UEs’ mobility to dynamically adapt to changing layouts. The result is a system that performs a smart interference coordination via the cooperation of MARL agents, adjusting transmission beams to follow moving UEs and adapting to intermittent blockages generated by random obstacles. To the best of our knowledge, no other works in literature deal with adaptive joint flow routing and link scheduling, via RL, in mmWave IAB networks whose dynamics are caused by both random link obstructions and UE mobility.

Our contributions are summarized as follows:

- We investigate the problem of joint flow routing and link scheduling in mmWave IAB networks to maximize the user throughput, taking into account intermittent links due to user mobility and mobile 3D obstacles.
- We exploit the distributed nature of the problem and propose an MARL-based approach that splits a combinatorial resource allocation problem into multiple small problems managed by cooperative agents. This allows to execute resource allocation operations that adapt in real-time to network and environment conditions.

- We propose an approach that coordinates the interference among concurrent backhaul and access links and monitors buffer levels at IAB-nodes to avoid the starvation of access transmissions due to empty relay buffers.
- We design different MARL settings for the cases where IAB-nodes respectively operate in full-duplex (FD) or half-duplex (HD) modes.
- We provide a communication and coordination scheme for RL agents, which enables the practical implementations of online training procedures in real systems.
- We conduct extensive numerical experiments to evaluate the proposed approaches and show how they outperform traditional resource allocation approaches.

The rest of the paper is organized as follows. We first discuss related works in Section 2, then we provide a system overview in Section 3. In Sections 4 and 5, the proposed approaches are detailed, while implementation issues are discussed in Section 6. The results of the numerical evaluation are showcased and discussed in Section 7. Finally, Section 8 concludes the article with some final remarks.

2 RELATED WORK

Resource management in multi-hop mmWave networks has been largely investigated in the recent literature, mainly facing the new challenges brought in by highly directional transmissions. Among all these works, the traffic routing and transmission scheduling problem has been carefully investigated [4–6]. However, only a few of them do consider the link status (i.e., line-of-sight (LOS), non-LOS (NLOS), outages, etc.). The works [7, 8] find routing paths to bypass the links interrupted by obstacles. The work in [9] performs a slot-by-slot link scheduling to maximize the instantaneous throughput considering link blockage probabilities described as a discrete-time Markov chain. Authors in [10] deal with the relay selection and link scheduling problem to maximize the end-to-end throughput, using 3D models of buildings as primary blockage sources. In [11], heuristic algorithms for user scheduling and power allocation are proposed to reduce outage occurrences.

Most of the studies on mmWave communications consider users’ mobility only in handover / user-cell association problems [12, 13]. Only a few works cope with user mobility when addressing resource allocation problems, but none of them deals with multi-hop networks. The work in [14] proposes a contextual multi-armed bandit algorithm to schedule transmissions to users with unknown positions. In [15], Deep Q-Network (DQN) is exploited to allocate capacity for up/down link transmissions in a 5G heterogeneous network with high-mobility. Authors in [16] select routing paths based on the mobility and traffic conditions, then they perform a link-resource time sharing according to flow occupations. A particle swarm optimization (PSO) algorithm is described in [17] to properly manage unmanned aerial vehicle (UAV) in mmWave aerial access and backhaul networks to serve mobile users. In [18], a band and beam allocation scheme for mmWave networks is presented, which considers massive-MIMO systems and user trajectories.

Recent years have witnessed a widespread utilization of Reinforcement Learning (RL) techniques in mmWave networks. A large part of the works in the literature deal with throughput maximization. The work in [19] defines a spectrum allocation for IAB networks that maximizes the sum of log-rates through double DQN and actor critic techniques. Authors in [20] resort to regret RL and successive convex approximation to perform route selection and rate allocation, respectively. Risk-sensitive RL is adopted in [21] to control transmitter beamwidth and power so as to maximize data rate. In [22], the authors propose a resource allocation framework based on advantage actor critic and column generation to maximize the throughput of mmWave IAB networks.

Some of the other works investigate latency performances. Link scheduling approaches based on deep deterministic policy gradient (DDPG) [23] and multi-armed bandit [24] are proposed to minimize the end-to-end latency in mmWave backhaul networks. Interference management and capacity issues have been faced as well. The work in [25] allocates capacity between the core network and mmWave BSs to users subject to blockages. Authors in [26] mitigate the inter-beam inter-cell interference through joint user-cell association and selection of number of beams. Finally, MARL emerges as a promising approach to cope with traffic signal control [27] and resource allocation [28] in vehicular networks, user association [29] and handover management [30] in mmWave networks.

The above works show several good examples of the interesting problems arising in mmWave networks as well as the potential of RL techniques in dynamic scenarios. However, none of them deals with the complexity and the entire set of features of the problem of adaptive flow allocation and link scheduling in mmWave IAB networks, characterized by access and backhaul transmissions, whose dynamics are caused by both intermittent links and UE mobility. To provide high user throughput, we propose a multi-agent RL approach able to properly coordinate interference among links concurrently activated and, at the same time, take into account the status of IAB-node queues. In this article, we extend the work in [31], which considers simplified sector-based blockage model and star-topology backhaul, by introducing a realistic link obstruction model relying on 3D mobile obstacles, a general tree-topology backhaul, and both full-duplex and half-duplex working modes at IAB-nodes.

3 SYSTEM MODEL

We consider a mmWave IAB network that consists of a mmWave base station (BS), *IAB-donor*, connected to the core network with a wired connection, and a set of small mmWave BSs, *IAB-nodes*, wirelessly backhauled to the IAB-donor using mmWave frequencies. A mobile user equipment (UE) gets access to the network via either a direct mmWave link connected with the IAB-donor or multiple hops through IAB-nodes. A typical example of the IAB scenario is depicted in Fig. 1. Backhaul links are established either between the IAB-donor and an IAB-node or between two IAB-nodes, while access links connect IAB-donor / IAB-nodes to UEs. Both backhaul and access communications

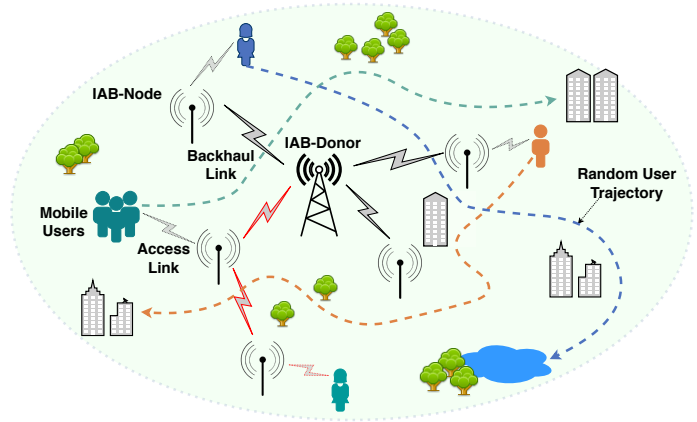


Fig. 1: An IAB network scenario with the trajectories of some mobile UEs.

share the same mmWave frequency band (i.e., in-band backhaul).

This scenario can be represented as a graph $\mathcal{G}(\mathcal{V}, \mathcal{E})$ where the node set \mathcal{V} is composed of an IAB-donor, IAB-nodes and UEs, and the edge set \mathcal{E} comprises all the potential links among the nodes. \mathcal{V} can be further divided into the set of IAB-nodes \mathcal{R} and the set of UEs \mathcal{U} . If not differently specified, the IAB-donor is identified as a special IAB-node. We consider a tree topology for the backhaul, where IAB-nodes are connected to the IAB-donor either directly or via multiple hops, as indicated in 3GPP specifications for IAB network simulations [32], which assume no more than 10 IAB-nodes organized in simple topologies.

3.1 Channel Access

The time domain \mathcal{T} is divided into frames, each of which consists of T slots with equal length δ . The system follows a space-division multiple access (SDMA) scheme to take advantage of the high directivity of mmWave antennas, allowing multiple concurrent transmissions involving both backhaul and access links to be carried out in each slot. Simultaneous activation of several links requires the network to satisfy several physical requirements, such as channel conditions (e.g., interference levels, antenna patterns), duplex communication modes (i.e., full-duplex, half-duplex), hardware and radio frequency (RF) chain limitations. We study the network performance regarding the downlink traffic transfer from the IAB-donor to UEs when all the IAB-nodes operate either in half-duplex (HD) mode (i.e., either receiving or transmitting in the same slot) or in full-duplex (FD) mode (i.e., able to simultaneously receiving and transmitting data). In HD mode, each antenna consists of side-by-side array panels where transmission (Tx) and reception (Rx) share the same panel and each panel is equipped with a single RF chain. In FD mode, each antenna consists of side-by-side pairs of separate Tx and Rx array panels [33], each of which is installed with a single Tx or Rx RF chain. Interference between incoming and outgoing links of an IAB-node operating in FD mode is assumed to be negligible thanks to ideal self-interference cancellation and

isolation techniques¹. Finally, a UE can receive from at most one IAB-node / IAB-donor in a slot.

A signal-to-interference-plus-noise ratio (SINR) model is used to establish a successful link: a connection is created only if the SINR at the receiver is larger than the threshold required by the selected modulation and coding scheme (MCS). The interference that one link receives from other transmitters is the sum of the power it receives from all the non-intended transmitters simultaneously activated. We consider rate adaptation where transmission rates depend on selected MCSs, which in turn depend on achievable SINR values.

We adopt common path loss and antenna pattern models [34, 35] for mmWave communications. The path loss model for line-of-sight (LOS) transmission is defined as:

$$PL_{dB} = \alpha + k \cdot 10 \cdot \text{Log} \left(\frac{d}{d_0} \right), \quad (1)$$

where $\alpha = 82.02dB$ and $d_0 = 5m$. d is the path length. The propagation factor k is 2.36 if $d > d_0$ and 2 otherwise. The antenna gain is modeled with a Gaussian main lobe profile:

$$G_{dB}(\phi, \theta) = 10 \cdot \text{Log}(G_0) - 12 \cdot \frac{\phi^2}{\phi_{-3dB}^2} - 12 \cdot \frac{\beta^2}{\beta_{-3dB}^2}, \quad (2)$$

$$G_0 = \frac{16\pi}{6.76 \cdot \phi_{-3dB} \cdot \beta_{-3dB}}. \quad (3)$$

ϕ_{-3dB} and β_{-3dB} are respectively the elevation and azimuth half power beamwidths (HPBW). The ϕ and β are the elevation and azimuth angle offsets between the main lobe direction and the direction to the considered transmitter/receiver. We assume omni-directional reception at UEs due to the typically limited hardware capabilities.

We would like to remark that the above models are just reasonable choices to obtain realistic scenarios, and thus, meaningful numerical results. Indeed, the approach we propose can be applied to any specific channel and antenna pattern model.

3.2 Blockage and Mobility Model

In this work, we consider UEs that move within the service area and links that can be suddenly blocked by unexpected obstacles. We adopt the well-known Random Waypoint model [36] for UE mobility, while obstacle blockages are modeled as follows.

Since mmWave signals can be strongly affected by obstacles, which generate link interruptions, and UEs mobility requires to consider dynamically established links, we have developed a dynamic and realistic blockage model. IAB-nodes are expected to be installed at relatively high places (e.g., lamp posts, roof tops, etc.) to improve visibility and avoid tampering, thus we deem that backhaul links are less likely to be blocked. In contrast, access links are exposed to more recurrent blockages caused by nomadic obstacles (e.g., pedestrian, transportation traffic, etc.). Based on the above

1. Since self-interference cancellation technique is out of scope of this paper, we just make this assumption in the experiments to obtain numerical results. However, our work can be applied even if self-interference in any form is included.

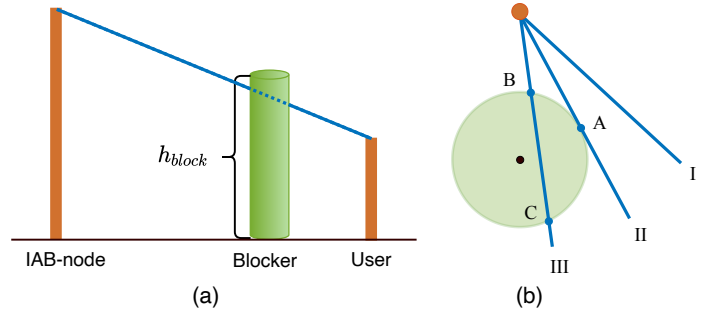


Fig. 2: 3D blockage model.

observation, we realistically apply blockages only to access links².

We consider 3D mobile obstacles (blockers) [37] that, like UEs, move around in the simulation field according to a Random Waypoint model. Fig. 2(a) illustrates how the blockage occurs. The obstacle is modeled as a cylinder standing in the LOS path between the transmitter and the receiver. Fig. 2(b) shows the corresponding top view where the intersection points between the LOS path and the blocking cylinder are identified as A , B and C , having respectively heights h_A , h_B and h_C . To determine whether a link blockage occurs, the following cases, represented in Fig. 2(b), are examined:

- Case I: when LOS path is neither a secant nor a tangent of the blocker's cross-section, there is no blockage in the transmission.
- Case II: when LOS path is a tangent of the blocker's cross-section, if $h_A \leq h_{block}$, the blockage occurs; otherwise, no blockage occurs.
- Case III: when the LOS is a secant of the blocker's cross-section. A blockage occurs only if $h_B \leq h_{block}$ or $h_C \leq h_{block}$.

Every time an obstacle interrupts an access transmission, the UE cannot receive any bits from the IAB-node, while the path loss model in Eq. (1) is applied if a link is not affected by obstacles.

UEs can move in the scenario with arbitrary directions and speeds, and they may undergo link blockages caused by random mobile blockers. This makes access links short-lived and unstable, thus posing a big challenge to resource allocation problems, especially to those based on traditional optimization techniques [22]. Indeed, these techniques rely on static assumptions and usually require a non-negligible amount of time to provide an optimal solution for a single network snapshot. Therefore, they cannot be applied to dynamic scenarios.

Thanks to the capability of learning dynamic statistics, RL is an appropriate tool to provide a practical and adaptive scheduling approach in such a complex and dynamic network environment. In particular, MARL techniques will allow us to split the problem into simpler tasks that multiple agents can perform by relying on local observations of the environment.

2. Note that this is not a limitation of our scenario, but rather an effort to make it more realistic. Indeed, backhaul link blockages can be straightforwardly included in the approach if a specific use case needs it.

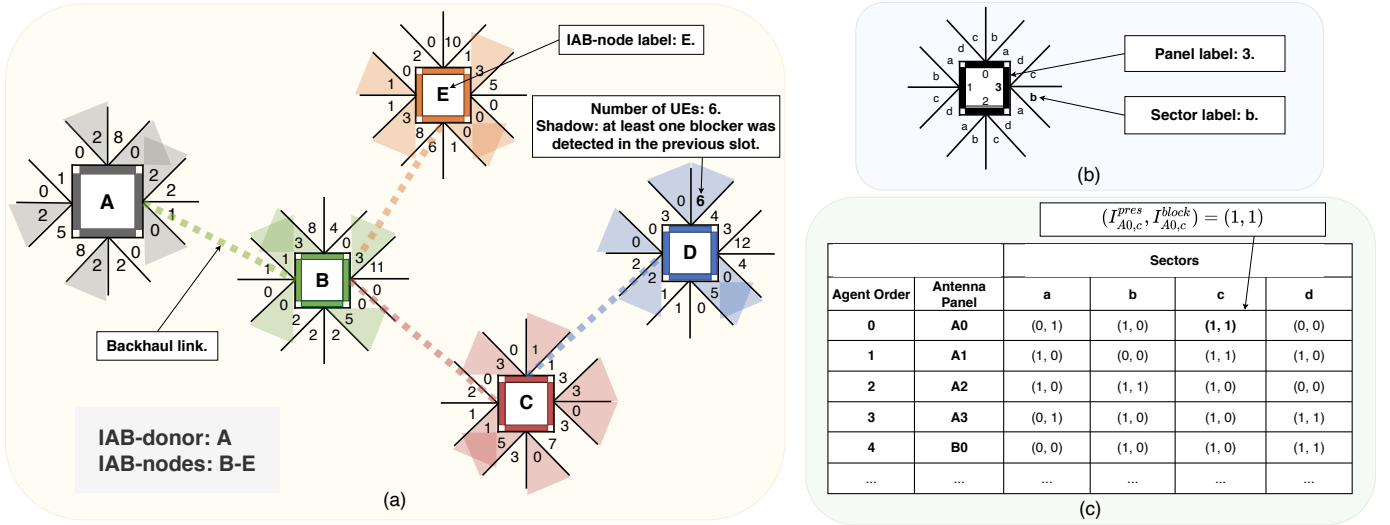


Fig. 3: An example of IAB scenario. (a) shows an IAB network with 1 IAB-donor and 4 IAB-nodes. Backhaul links (dashed lines) form a tree topology and the number of covered UEs is reported in each sector. A sector is shadowed if at least a mobile blocker has been detected in the previous slot. (b) is the top view of an IAB-node equipped with 4 Tx/Rx array panels, each of which manages 4 sectors (a, b, c, d). (c) includes a table reporting the binary information expressing UE presence and blockage conditions in the layout shown in (a).

3.3 Network Operations

Access Links: UEs connecting to mmWave IAB networks are expected to work in dual-connectivity mode [38]. Indeed, user devices will be equipped with both legacy (i.e., 3GPP FR1) and mmWave (3GPP FR2) interfaces. It is arguable that control-plane information will be exchanged through the legacy FR1 interfaces of such architecture, in order to provide better coverage and signal propagation conditions. Instead, high-throughput user-plane channels can be established, when available, through mmWave links. In addition, the control-plane FR1 interface can be used to send UE context information to enable better network access point selection and configuration. Under these conditions, we can reasonably assume that each IAB-node is informed about associated UEs in real time, and in particular, about their positions, channel conditions, collision occurrences, etc.

Considering realistic nodes as shown in Fig. 3(b), each Tx panel covers a 180° area, which is divided into N_s sectors that indicate the possible beam directions. Every time a beam is pointed to a specific sector, a UE, if any, is served. If more than one UE is present, one of them is randomly selected as the intended receiver. A collision occurs if a UE is selected as the receiver from more than one panel in the same time slot. Whenever it occurs, no bit can be delivered to the UE. Finally, if an access link is blocked by any obstacle, the data transmission fails. Fig. 3(b) provides a top view of a node. The node is equipped with 4 Tx array panels (0, 1, 2, 3) and each panel (agent) manages 4 angular sectors (a, b, c, d). Fig. 3(a) shows an IAB wireless backhaul where 4 IAB-nodes are connected to an IAB-donor in a tree topology. Each sector of each panel is marked with the number of UEs under its coverage and shadowed if any access link in it was obstructed in the previous slot.

Backhaul Links: As for the backhaul transmissions, we assume they are carried out through pairs of IAB-donor-IAB-node or IAB-node-IAB-node panels. The two endpoints

of each link focus each other using the reciprocal sector and panel whose pointing direction is the closest to the one of the LOS segment, as shown in Fig. 3(a) with dashed lines. Therefore, each child IAB-node of the tree topology is associated with a sector of a panel at the IAB-donor or at its parent IAB-node.

Node Buffers: Each IAB-node has a queue (buffer)³ storing bits received via backhaul links from the IAB-donor or its parent IAB-node. The buffer is shared among all the panels of the IAB-node. Therefore, the throughput eventually delivered to other IAB-nodes or UEs depends not only on the link capacities defined by SINR values, but also on the number of available bits in the buffers. This requires to monitor buffer levels at IAB-nodes, which must be timely refilled to avoid any impact on downstream transmissions.

In our approach, each IAB-node informs its parent node about its buffer level at each time slot. Based on the buffer levels of its child IAB-nodes, a parent IAB-node/IAB-donor – more specifically, the connected RL agent – will have to choose to send data bits to an IAB-node via a backhaul link, to refill its buffer, or directly to a UE via an access link, to improve its throughput. When IAB-nodes operate in HD mode, if an IAB-donor/IAB-node selects to refill a child IAB-node’s buffer in a specific slot, the child IAB-node cannot carry out any transmission in the same slot. Vice versa, if IAB-nodes operate in FD mode, they can always transmit regardless they are receiving or not from their parent nodes. Finally, in both FD and HD modes, an IAB-node can receive from at most one transmitter in each time slot, by using any of its Rx panels.

3. We assume that buffer sizes do not limit the performance of the system. However, queue limits can be easily added to the RL environment and RL agents can be trained accordingly.

4 ADAPTIVE ROUTING AND LINK SCHEDULING VIA MARL

RL was born as a tool to optimize decision-making and control through the experience accumulated by an agent during sequential interactions with an environment, following a trial-and-error strategy. Specifically, at step t , conditionally to the state $s_t \in \mathcal{S}$ of the environment, the agent selects an action $a_t \in \mathcal{A}$ according to its current policy π and executes it in the environment. At step $t + 1$, based on its reaction to a_t , the environment switches to state s_{t+1} and gives a reward r_t back to the agent. When states are partially-observable, an agent can only collect an observation $o_t \in \mathcal{O}$, which contains partial information of the global state s_t . Therefore, its policy π will select an action a_t conditional to current observation o_t . During the interactions, the agent adjusts the policy π so as to maximize the long-term cumulative reward, namely the *expected return* $\mathbb{E}_\pi[G_t] = \mathbb{E}[\sum_{k=t+1}^{\infty} \gamma^{k-t-1} r_k]$, where γ is a discount factor controlling the importance of a future reward to the current utility.

A first approach to apply RL to IAB networks is to consider a central network controller that acts as a single RL agent. However, this requires the agent to know the global state of the whole network and manage all the transmissions, resulting in combinatorially large numbers of different states and possible actions, which will increase exponentially with the size of the network. This would strongly limit the scalability and flexibility of the approach, which can be even aggravated by the system dynamics due to the UE mobility. These reasons motivated us to resort to a Multi-Agent RL (MARL) approach in our framework, which allows to split the overall complexity into several smaller problems managed by cooperative agents. Cooperation is fundamental, as directly applying independent Single-Agent RL (SARL) algorithms to each individual agent to maximize its own return leads to poor results. Indeed, interpreting other agents' decisions as part of the environment would make it non-stationary as other agents' policies constantly update. This produces ineffective learning.

In our MARL approach, we consider multiple RL agents and assign one of them to each of the N_p panels installed at an IAB-node (or at the IAB-donor), such that each agent can control the beamforming of the panel at each time slot. Each panel (RL agent) cooperates with other panels to learn the dynamics of the environment and understand the impact of the other panels' policies.

The collective goal of the agents is to maximize the throughput (namely, the number of bits per frame) delivered to UEs. This requires a proper management of the backhaul and access link transmissions during a frame. How to achieve high UE throughput without significantly reducing fairness depends on how RL agents (antenna panels) point their beams, which IAB-node buffer is selected to be refilled, and how data bits flow through the network, crossing IAB-nodes. One time slot of the frame corresponds to one step of RL interactions, that is, each agent executes an action at each slot, according to the policy π available at the beginning of the slot. Two types of actions are possible for each agent: either transmitting over a backhaul link towards an associated (covered) IAB-node or activating a specific

sector to serve a UE through an access link. As long as an action is selected, the total number of bits transmitted in a slot by an IAB-node is limited by either the number of bits in its buffer or the link capacity achievable with the actual SINR value.

4.1 RL Formulation

Considering $|\mathcal{R}|$ IAB-nodes (including the IAB-donor), each equipped with N_p antenna panels, provides a total of $N = |\mathcal{R}| \cdot N_p$ agents, indexed by $\mathcal{I}_p = \{1, \dots, N\}$. Each panel (agent) faces N_s sectors indexed by $\mathcal{I}_s = \{1, \dots, N_s\}$. The observation space \mathcal{O} , action space \mathcal{A} , and reward function of the RL agents are defined as follows, considering IAB-nodes operating in FD and HD modes.

4.1.1 Observation Space

Since IAB-nodes can work in FD and HD modes, we design different observations accordingly. They contain a mode-specific element and several other common elements.

Full-duplex Mode: For each agent (panel) p , the observation includes the binary information of:

- 1) *UE presence* - $I_{p,s}^{pres}$, which takes value 1 for sector s of agent (panel) p if there are UEs located under the coverage of sector s . This information can be easily estimated by using signaling and context information (e.g., position, received power, etc.) sent by UEs.
- 2) *Sector blockage* - $I_{p,s}^{block}$, which takes value 1 if sector s of agent (panel) p encountered a blockage in the previous slot (i.e., the previous transmission carried out in sector s failed). Blockers moving at realistic speed can lead to sector (beam) obstructions that last hundreds, or even thousands, of slots and suddenly disappear in few slots with the departure of the blockers [39]. A similar behavior repeats in the opposite transition from blocked to free sectors. Therefore, the blockage status in the previous slot is the optimal predictor for all the slots but those experiencing a transition, which are limited in number and whose occurrence instants are very hardly predictable in any case. An example of the above binary information vectors is shown in Fig. 3(c).
- 3) *Child-node buffer level* - L_n , which indicates the number of bits in the buffer of child IAB-node n , reachable through panel p . Since we are interested in defining a policy that maximizes the UE throughput, we assume full-buffer conditions for the IAB-donor. As for IAB-nodes, instead, their buffer-level information is essential for parent IAB-donor/IAB-node agents to plan their buffer-refilling strategies.

The above information is organized in concatenated sub-vectors to form an observation vector for agent $p \in \mathcal{I}_p$ that is collected at each RL iteration. Namely, we have:

$$o_p = [[I_{p,s}^{pres}]_{s \in \mathcal{I}_s}, [I_{p,s}^{block}]_{s \in \mathcal{I}_s}, [L_n]_{n \in \mathcal{R}_p}], \quad (4)$$

where \mathcal{R}_p is the set of child IAB-nodes reachable via panel p .

Half-duplex Mode: All the previous three sub-vectors also appear in the observation vector of the HD mode. However, differently from FD mode, operating in HD mode introduces synchronization issues between parent and child nodes: if a parent node transmits to a child node, the receiving child node cannot simultaneously transmit. This may

hinder the data delivery in the tree topology where data bits require multiple backhaul hops to reach UEs. This poses a big challenge to the cooperation of RL agents, which have to coordinate several concurrent and dynamic factors (i.e., interference reduction, buffer refill and collision avoidance).

Therefore, we add a fourth sub-vector, $[B_n]_{n \in \mathcal{R}_p}$, to the observation vector, which indicates the number of bits transmitted downstream in the current slot by every child IAB-node n reachable through the panel p ($n \in \mathcal{R}_p$). This information, together with L_n , allows the parent agent to balance between the buffer level and the transmission opportunity of each child node in order to avoid empty buffers and provide a good downstream throughput. As a result, the observation vector of the agent $p \in \mathcal{I}_p$ working in HD mode is:

$$o_p = [[I_{p,s}^{pres}]_{s \in \mathcal{I}_s}, [I_{p,s}^{block}]_{s \in \mathcal{I}_s}, [L_n]_{n \in \mathcal{R}_p}, [B_n]_{n \in \mathcal{R}_p}] \quad (5)$$

4.1.2 Action Space

Each agent $p \in \mathcal{I}_p$, working in the HD or FD mode, can choose to (1) activate one of its N_s sectors to transmit to a covered UE (*ACC* action), to (2) transmit to one of the reachable IAB-nodes in set \mathcal{R}_p (*BH* action), or to (3) stay silent (*SIL* action).

Using sector-based transmissions in (1) allows to reduce the impact of the UE location, which changes over time, on action policies, making them more stable and robust against mobility. In addition, this permits the same action space to remain widely applicable even if the number of UEs in the service area is not constant. Indeed, once a sector is selected, only one UE, if any, will be randomly selected to be served.

In each slot, every agent tries to establish a link according to the selected action: activating a sector or connecting to an IAB-node. Concurrent links interfere with each other and can transfer a number of bits which depends on the actual SINR value. Whether or not activated links can truly deliver that number of bits finally depends on whether IAB nodes have enough bits buffered or an obstacle produces a blockage. If buffer level is the limiting factor, fairness is pursued by equally sharing buffered bits among the links simultaneously activated. If an obstacle is present, no bit can be delivered. The coordination among agents aims at maximizing the number of bits transferred to UEs, which is obtained by finely tuning the following rewards.

4.1.3 Reward Function

We have designed two reward functions for FD and HD, respectively. Similarly to the definition of the observation space, the reward for the HD case shares some common elements with the one for the FD case and has an additional element to prevent IAB-node starvation.

Full-duplex Mode: Each agent (panel) can either (1) activate an access link, or (2) transmit along a backhaul link, or (3) stay silent. According to these actions, three types of reward must be designed.

If agent p plays (1) and succeeds in serving a UE, it gets a positive reward equal to the number of bits B_p sent by the panel p , multiplied by $(h(p) + 1)$, where $h(p)$ is the number of hops separating the agent p 's IAB-node from the IAB-donor, and normalized by c_{min} , the minimum capacity (minimum MCS) available in the whole network.

Note that the factor $h(p)$ leads to higher rewards to transmissions serving UEs farther away from the IAB-donor. This allows to efficiently use the resources of the backhaul network rather than relying on the myopic delivery of traffic only to nearby UEs, directly connected to the IAB-donor.

If agent p plays (2) and successfully transmits data via a backhaul link, similarly to the case of an access transmission, the reward is computed as the number of sent bits B_p normalized by c_{min} and multiplied by $(h(p) + 1)$. In addition, the fraction is further multiplied by a weight $\rho_{BH} \in (0, 1)$ that is used to counterbalance the fact that the backhaul link capacity, and thus the number of transferred bits, is usually remarkably larger than access link capacity. Without ρ_{BH} , agents would largely prefer to activate backhaul links, accumulating data bits in IAB-nodes' buffers.

When agent p plays (3), there are two types of outcomes. 1) The buffer of the IAB-node where p is installed is empty, which is an external limitation not directly ascribable to the agent's policy (namely, the panel p belongs to the set of panels with empty buffer, $p \in \mathcal{I}_p^{EB}$). Therefore, the reward is set to 0 to prevent the agent's training process from being biased by its empty queue. 2) If agent p , despite having bits in the buffer, selects to stay silent, it gets a penalty $-\zeta$ (empirically, $\zeta = 1$) in order to incentivize policies that increase the throughput. Similarly, if agent p has bits and its transmission experiments a blockage or a collision, it will get a penalty $-\zeta$ for its neglecting the obstacles or not cooperating well with the other partner agents.

Therefore, the reward of agent p working in FD mode is:

$$r_p = \begin{cases} \frac{(h(p)+1) \cdot B_p}{c_{min}}, & \text{if } B_p > 0, p \notin \mathcal{I}_p^{EB}, \text{ACC act.}, \\ \rho_{BH} \cdot \frac{(h(p)+1) \cdot B_p}{c_{min}}, & \text{if } B_p > 0, p \notin \mathcal{I}_p^{EB}, \text{BH act.}, \\ 0, & \text{if } p \in \mathcal{I}_p^{EB}, \\ -\zeta, & \text{otherwise.} \end{cases} \quad (6)$$

Half-duplex Mode: The reward function of an agent p working in HD mode is the same as the one of a FD agent, except for two aspects.

For a backhaul transmission to an IAB-node n , the agent p gets a reward computed in the same way as in FD case, but additionally scaled by the number of bits L_n in n 's buffer after the reception. This additional scaling factor gives smaller rewards to the transmissions to nodes with more bits in the buffer. This helps to avoid both parent-node transmissions that prevent child nodes from transmitting downstream and large deviations in the buffer levels of different IAB-nodes.

When agent p does not transmit any bit, the reward is set to 0 not only if the IAB-node's buffer is empty ($p \in \mathcal{I}_p^{EB}$), but also if the IAB-node is receiving data from a parent node in the same slot ($p \in \mathcal{I}_p^{RX}$). To simplify the notation we define $\mathcal{I}_p^{ER} = \mathcal{I}_p^{EB} \cup \mathcal{I}_p^{RX}$. Therefore, the reward of agent p working in HD mode is written as follows.

$$r_p = \begin{cases} \frac{(h(p)+1) \cdot B_p}{c_{min}}, & \text{if } B_p > 0, p \notin \mathcal{I}_p^{ER}, \text{ACC act.}, \\ \rho_{BH} \cdot \frac{(h(p)+1) \cdot B_p}{c_{min} \cdot L_n}, & \text{if } B_p > 0, p \notin \mathcal{I}_p^{ER}, \text{BH act.}, \\ 0, & \text{if } p \in \mathcal{I}_p^{ER}, \\ -\zeta, & \text{otherwise.} \end{cases} \quad (7)$$

5 LEARNING APPROACH

In this section, we detail the learning process for RL agents, whose components have been described in the previous section. We first introduce some preliminaries about the single-agent RL techniques, then we present our multi-agent learning approach, followed by a discussion on communication and coordination aspects.

5.1 Actor and Critic

The goal of an RL agent is to adjust its policy π so as to maximize its *expected return* $\mathbb{E}_\pi[G_t] = \mathbb{E}[\sum_{k=t+1}^{\infty} \gamma^{k-t-1} r_k]$.

A first type of learning approaches resort to an action-value function $Q(s_t, a_t) = \mathbb{E}_\pi[G_t | s_t, a_t]$ that corresponds to the expected return from state s_t , taking action a_t and following policy π afterwards. An RL agent iteratively estimates this action-value function and selects at each step the action with the maximum function value in the current state. This is the fundamental idea of *value-based* RL approaches. $Q^\psi(s_t, a_t)$ can be approximated as a ψ -parametric function of state and action, which can take the form of a deep neural network (DNN) with weights ψ . Parameters ψ can be estimated via temporal-difference approaches by minimizing the regression loss $\mathcal{L}_Q(\psi) = \mathbb{E}_{(s_t, a_t, r_t, s_{t+1}) \sim H} [(Q^\psi(s_t, a_t) - y)^2]$, where $y = r_t + \gamma \mathbb{E}_{a_{t+1} \sim \pi(s_{t+1})} [Q^\psi(s_{t+1}, a_{t+1})]$ is the updated return, Q^ψ is a moving average of the past Q functions, and H is a replay buffer storing past agent-environment interaction data tuples, including states, actions, and rewards.

A second family of learning techniques solve the problem from a different perspective, which are called *policy-gradient* RL approaches. They see a policy as a function indicating the probability of selecting action a_t in state s_t , parameterized with vector θ , $\pi_\theta(a_t | s_t) = \text{Pr}_\theta\{a_t | s_t\}$, which can be represented by a DNN as well, with θ as connection weights. Parameters θ are updated by applying approximate gradient ascent to $\mathbb{E}[G_t]$, thus considering $\nabla_\theta \mathbb{E}[G_t]$, whose unbiased estimate is $\nabla_\theta \log \pi_\theta(a_t | s_t) G_t$. In addition, G_t can be approximated by its expectation $\mathbb{E}_\pi[G_t | s_t, a_t]$, which corresponds to the action-value function $Q^\psi(s_t, a_t)$. To reduce the estimate variance during updates, a state-dependent baseline $b(s_t)$ value is often subtracted from the unbiased estimate: $\nabla_\theta \log \pi_\theta(a_t | s_t) (Q^\psi(s_t, a_t) - b(s_t))$, where $Q^\psi(s_t, a_t) - b(s_t)$ is the *advantage* of selecting action a_t over the other actions at state s_t .

The previous two paragraphs briefly outlined the basics of *Actor-Critic* technique [40], which is emerging as one of the best-performing RL approaches as it is derived from a policy-gradient approach, but incorporates the strength of a value-based approach. In particular, the *critic* part estimates the action-value function based on past interactions, thus generating the values of $Q^\psi(s_t, a_t)$, while the *actor* part updates the policy $\pi_\theta(a_t | s_t)$ according to the gradient direction, which in turn depends on the action-value function generated by the critic⁴. Note that when considering partially-observable situations, the policy becomes $\pi_\theta(a_t | o_t)$, which maps partial observation o_t into a

4. Following the convention in Actor-Critic techniques, we will interchangeably refer to, respectively, critic or action-value function Q and actor or policy function π in the remainder of the article.

probability distribution over the action set. Similarly, the action value function becomes $Q^\psi(o_t, a_t)$.

5.2 Multi-Agent Learning

The approach we propose in this article is based on the Multi-Actor-Attention-Critic (MAAC) [41] technique that allows to train multiple agents to pursue a collective goodness. MAAC has two remarkable advantages: (1) its critic part allows each agent to automatically consider observations and actions only from relevant agents (based on the idea of *attention*), thus filtering out information not correlated to a performance improvement; (2) it trains decentralized policies with centrally-computed critics, which allows agents to use individual policies and independently apply them, once training is completed. Therefore, we have adapted this technique to our scenario.

The centralized critics can be computed at a central entity located at the IAB-donor, while actors are installed at IAB-nodes and associated to antenna panels. The distributed architecture relies on message exchanges between the IAB-donor and IAB-nodes through direct control-plane links, which can be established at FR1 frequencies. Message exchanges are required only during the training phase, leaving the operation phase with fully distributed policies. Note that, as we will show in the following, only a limited amount of information has to be exchanged during training to achieve good results. Considering our MARL-based approach, its architecture can be seen in Fig. 4(a).

Denoting observations, actions, rewards and policy parameters of all the N agents as respectively $o = (o_1, \dots, o_N)$, $a = (a_1, \dots, a_N)$, $r = (r_1, \dots, r_N)$ and $\theta = (\theta_1, \dots, \theta_N)$ ⁵, the key idea of MAAC is to train each agent i 's individual policy $\pi_{\theta_i}(a_i | o_i)$ by means of its action-value $Q_i^\psi(o, a)$. The value of $Q_i^\psi(o, a)$ is centrally computed by using information from other relevant agents, according to the attention mechanism. Therefore, agent i 's $Q_i^\psi(o, a)$ depends not only on its own observation o_i and action a_i , but also on those of the other agents. It takes the following form:

$$Q_i^\psi(o, a) = f_i(e_i(o_i, a_i), x_{\setminus i}), \quad (8)$$

$$x_{\setminus i} = \sum_{j \neq i} \omega_j \cdot g(e_j(o_j, a_j)), \quad (9)$$

where f_i consists of one fully connected layer with leaky ReLU non-linearity and one linear layer, while e_i is an embedding function implemented as a fully connected layer with leaky ReLU. The contribution $x_{\setminus i}$ to agent i from the other agents is a weighted sum of functions of the other agents' embedding functions. In particular, g is a fully connected layer with leaky ReLU. Weight ω_j is the *attention weight* associated to the information provided by agent j , which is optimized during the training phase, together with the other weights of the neural network. The value of ω_j is computed according to a similarity value between e_i and e_j , which is computed using a matching approach between

5. To simplify the notation when dealing with multiple agents, we implicitly assume that observations, actions and rewards occur at time step t , f.i., $o \equiv o_t$. Instead, we use subscript i in o_i to indicate the observation at time t of the i -th agent. Observations occurring at time $t + 1$ are indicated as o' .

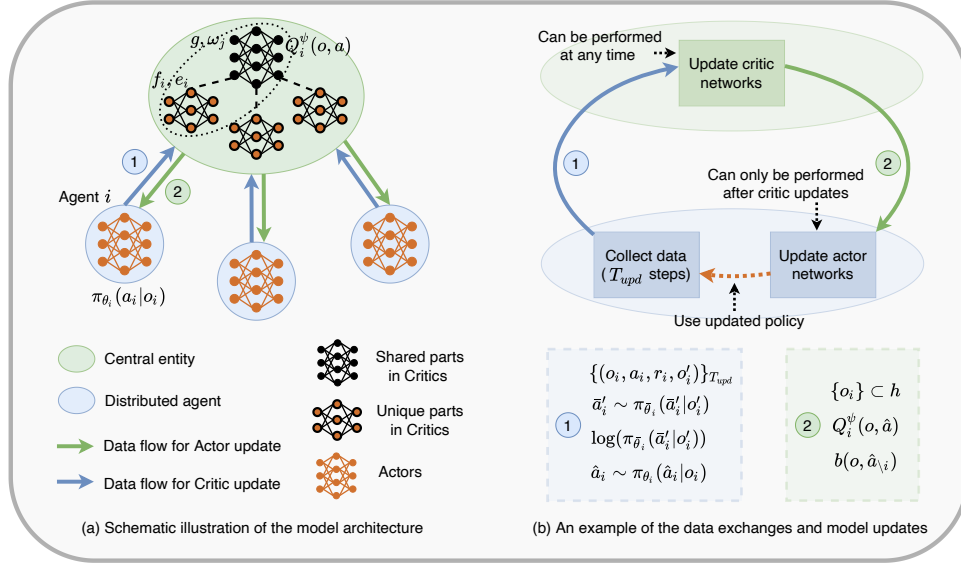


Fig. 4: Basic principle of the MARL framework. **(a)** Architecture overview of our approach, together with **(b)** the communication and coordination scheme in the training framework .

“query” based on e_i and “key” based on e_j (See [41] for further details). In Eqs. (8) and (9), f_i and e_i are *unique parts* to each agent, while g and ω_j are *shared parts* among all the agents. They can be visualized in Fig. 4(a). The centralized action-value function $Q_i^\psi(o, a)$ of agent i , encircled with a black dot line, includes the black shared critic NN and an orange black unique critic NN.

As mentioned before, functions and parameters in Eqs. (8) and (9) are implemented as DNNs, whose weight vector ψ is updated considering a replay buffer H that stores history trajectories in the form of (o, a, r, o') entries (o' is the next observation, resulting from the application of action a), which summarize the interactions occurred in the previous steps. In particular, based on a set of entries randomly sampled from the replay buffer, we update ψ to minimize the following joint regression loss function:

$$\mathcal{L}_Q(\psi) = \sum_{i=1}^N \mathbb{E}_{(o, a, r, o') \sim H} [(Q_i^\psi(o, a) - y_i)^2], \quad (10)$$

$$y_i = r_i + \gamma \mathbb{E}_{\bar{a}' \sim \pi_{\bar{\theta}}(o')} [Q_i^{\bar{\psi}}(o', \bar{a}') - \tau \log(\pi_{\bar{\theta}_i}(\bar{a}'|o'_i))], \quad (11)$$

where $Q_i^{\bar{\psi}}$ and $\pi_{\bar{\theta}}$, respectively called target action-value functions and target policies, are moving averages of the past action-value and policy functions (used to stabilize the training), while \bar{a}'_i is the next action that agent i would select by applying the target policy $\pi_{\bar{\theta}_i}$ to the next observation o'_i . The logarithmic term in Eq. (11) is called policy entropy. It encourages the exploration by promoting random selections, thus reducing the probability to converge to deterministic policies with poor local optima. Parameter τ is the trade-off weight used to balance the importance of the reward maximization over the random exploration. Finally, note that the evaluation of this loss function requires a joint optimization of ψ across all the individual action-value functions $Q_i^\psi(o, a)$, therefore it is performed at the central entity.

Once $Q_i^\psi(o, a)$ is updated using Eq. (10), the individual policy $\pi_{\theta_i}(a_i|o_i)$ of each agent i (shown as an orange actor

NN in Fig. 4(a)) can be updated as well, according to a gradient ascent approach over DNN weights θ_i :

$$\nabla_{\theta_i} J(\pi_\theta) = \mathbb{E}_{o \sim H, \hat{a} \sim \pi_\theta} \left[\nabla_{\theta_i} \log(\pi_{\theta_i}(\hat{a}_i|o_i)) \cdot \left(-\tau \log(\pi_{\theta_i}(\hat{a}_i|o_i)) + Q_i^\psi(o, \hat{a}) - b(o, \hat{a}_{\setminus i}) \right) \right]. \quad (12)$$

Each policy network with θ_i is composed of three linear layers and a final leaky ReLU non-linearity. The baseline $b(o, \hat{a}_{\setminus i})$ allows to reduce the variance of the gradient and is computed by averaging $Q_i^\psi(o, \hat{a})$ (i.e., $Q_i^\psi(o, (\hat{a}_i, \hat{a}_{\setminus i}))$) over all the possible actions of agent i (\hat{a}_i) according to the policy distribution π_{θ_i} , keeping fixed the actions of the other agents ($\hat{a}_{\setminus i}$). Note that the update of θ_i , although based on a per-agent action-value $Q_i^\psi(o, \hat{a})$, requires the knowledge of the other agents’ observations sampled from H and the other agents’ action probabilities expressed by π_θ .

6 COMMUNICATION AND COORDINATION SCHEME

Our MARL-based approach is characterized by per-agent policy functions $\pi_{\theta_i}(a_i|o_i)$ ($i \in \mathcal{I}_p$) based on DNNs that determine the actions of individual agents according to local observations. These policy functions must be tuned to the specific environment (i.e., node locations, blockage behavior, and user mobility), thus an initial training phase is needed to adjust DNNs’ weights. Once trained, each agent can select its action in isolation based on its own policy function and local observation, with no need to exchange data with other agents. Note that the training procedures can be re-activated at any point in time during the operation of the IAB system, f.i., periodically or when a substantial performance decrease is detected. The training cycle is shown in Fig. 4(b).

The training phase is based on the centralized update of the action-value functions $Q_i^\psi(o, a)$ ($i \in \mathcal{I}_p$) according to Eqs. (10) and (11). This task requires the central entity to have a centralized replay buffer H storing past experiences of all the agents.

During network operations, agent i plays action a_i at each step t , selected by using its own policy π_{θ_i} on the basis of its observation o_i . This leads to a reward r_i and a new observation o'_i . Each new tuple (o_i, a_i, r_i, o'_i) is temporarily and locally accumulated by each agent i which periodically sends a tuple batch $tup_i = \{(o_i, a_i, r_i, o'_i)\}_{T_{upd}}$ to the central entity considering the last T_{upd} steps. The central entity merges received tuples into vector tuples $\{(o, a, r, o')\}_{T_{upd}}$ and inserts them into the centralized replay buffer H used by the learning algorithm.

The batch update allows to perform DNN training in parallel to network operations. Indeed, when a concurrent training phase takes place, the actions performed during network operations will be selected according to the current (sub-optimal) version of the policy functions, which will be updated and improved after few interactions. Note that only the experience collected after the policy update will be sent to the central entity for the critic updates, as illustrated by the orange dashed arrow in Fig. 4(b), while other interactions are used to keep the IAB network in operation.

In each periodic update, the central entity samples a random mini-batch h from H consisting of a number h_{size} of vector tuples (i.e., $h = \{(o, a, r, o')\}_{h_{size}}$) and uses it in the minimization of the joint regression loss function (10) to update $Q_i^\psi(o, a)$ ($i \in \mathcal{I}_p$). Namely, for each vector tuple in h , the central entity updates ψ according to the following equations:

$$\mathcal{L}_Q(\psi) = \sum_{i \in \mathcal{I}_p} [(Q_i^\psi(o, a) - y_i)^2], \quad (13)$$

$$y_i = r_i + \gamma [Q_i^{\bar{\psi}}(o', \bar{a}') - \tau \log(\pi_{\bar{\theta}_i}(\bar{a}'|o'))]. \quad (14)$$

Note that, while mini-batch h is generated at the central entity, \bar{a}'_i and the value of $\log(\pi_{\bar{\theta}_i}(\bar{a}'_i|o'_i))$ are received from remote agents. After the update, target action-value functions $Q_i^{\bar{\psi}}$ ($i \in \mathcal{I}_p$) are updated using a moving average with an update rate κ .

The overall information sent by each IAB-node array panel (remote agent) i to the IAB-donor (centralized entity), shown by blue arrows ① in Fig. 4, is dominated by the set of the tuples $tup_i = \{(o_i, a_i, r_i, o'_i)\}_{T_{upd}}$. The size of a tuple is mainly determined by the size of an observation o_i , which consists of $2N_s + N_i^{ch}L$ bits for FD case and $2N_s + N_i^{ch} \cdot (L+B)$ bits for HD case, where $2N_s$ is given by the UE presence ($I_{i,s}^{pres}$) and sector blockage ($I_{i,s}^{block}$) bitmaps, L and B are respectively the numbers of bits used to indicate the buffer level and the amount of the delivered data, and N_i^{ch} is the number of child IAB-nodes connected to i , typically small (e.g., 2-4). Together with tuples, each IAB-node additionally sends for each tuple $t_i = (o_i, a_i, r_i, o'_i) \in tup_i$:

- action \hat{a}_i that it would play in front of current observation o_i in t_i , selected according to the current policy function $\pi_{\theta_i}(\hat{a}_i|o_i)$;
- action \bar{a}'_i that it would play in front of the next observation o'_i in t_i , selected according to its target policy function $\pi_{\bar{\theta}_i}(\bar{a}'_i|o'_i)$;
- the value of $\log(\pi_{\bar{\theta}_i}(\bar{a}'_i|o'_i))$, conditional to o'_i in t_i and according to the target policy function $\pi_{\bar{\theta}_i}(\bar{a}'_i|o'_i)$.

Actions \bar{a}'_i and the values of $\log(\pi_{\bar{\theta}_i}(\bar{a}'_i|o'_i))$ are used in the centralized action-value function updates according to

Eqs. (13) and (14), while \hat{a}_i is used at the central entity to compute $Q_i^\psi(o, \hat{a})$ and $b(o, \hat{a}_{\setminus i})$ that will be redistributed to all the agents to perform policy updates.

Once the $Q_i^\psi(o, a)$ ($i \in \mathcal{I}_p$) functions are updated, the central entity immediately sends to each agent i the needed information to update its policy (shown by green arrows ② in Fig. 4). In particular, the information includes:

- observation set $\{o_i\}_{h_{size}}$ derived from tuples in h ;
- the values of $Q_i^\psi(o, \hat{a})$ and $b(o, \hat{a}_{\setminus i})$.

Each agent i performs gradient ascent to update θ_i , as in Eq. (12), and obtains a new $\pi_{\theta_i}(a_i|o_i)$, which will be locally used in the next steps of the learning phase until an updated policy is generated. In practice, after new data are received from the central entity, agents' policy parameters are modified as follows:

$$\nabla_{\theta_i} J(\pi_\theta) = \nabla_{\theta_i} \log(\pi_{\theta_i}(\hat{a}_i|o_i)) \cdot \left(-\tau \log(\pi_{\theta_i}(\hat{a}_i|o_i)) + Q_i^\psi(o, \hat{a}) - b(o, \hat{a}_{\setminus i}) \right). \quad (15)$$

Note that action \hat{a}_i is the same as the one sent to the central entity, thus it is generated at agents before sending information to the central entity and then stored to be used for computing Eq. 15. As a final task, each agent updates its target policy with a moving average.

6.1 Dealing with the Temporal Dynamics

The communication and coordination scheme discussed above is based on DNN updates, which require interactions between the central entity at IAB donor and distributed agents at IAB nodes. The time between two updates directly impacts on the convergence speed, but it is potentially arbitrary. Indeed, it can be set according to the length of an arbitrary update episode, the time to process an update, or the replay-buffer sampling factor to generate a mini-batch. However, to strike a balance between model training efficiency and message exchange costs, a proper update interval needs to be set.

Theoretically, new information collected at the agents can be accumulated and sent to the central entity at any time. Likewise, critic updates can be performed at any time, when a sufficient number of new tuples have been inserted in the replay buffer. Policy updates at distributed agents, instead, must be performed only when new Q-function values are received from the central entity.

In addition, note that coordination information exchanges may be characterized by a non-negligible latency (e.g., T_l^A and T_l^C in Fig. 5), which introduces some delay between last-collected interaction tuples and DNN updates. This may not be a critical issue, as model updates are based on random samples of the past tuples included in the replay buffer H , thus they can be performed at arbitrary time points instead of waiting for the data arrival. However, we provide two possible training timelines to show the latency impact.

Solution 1. Updates can be triggered by the central entity as soon as it receives new tuples from remote agents, as illustrated in Fig. 5(a). It updates the central DNNs, then, sends new values to the agents, which update their policies.

Solution 2. Updates at the central entity and at distributed agents are performed periodically, based on timers.

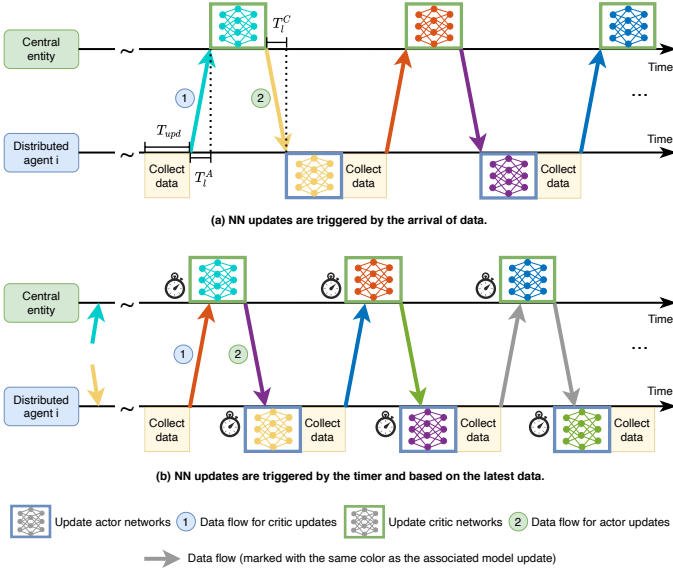


Fig. 5: An illustrative example of the transmission latency impact on the model training.

Central DNN updates are performed with data sampled from the most recent content of the replay buffer, while distributed agents' DNNs are updated with the latest data received from the central entity. Fig. 5(b) illustrates this idea, where colored DNNs' updates are based on the data transmitted through the arrows with the same colors. Compared with Solution 1, this solution allows to overcome the effect of transmission latency, thus accelerating the training process.

Finally, note that multiple DNN updates can be performed at each update time instant, by consecutively sampling K random mini-batches from the replay buffer and updating DNNs' weights according to the content of each of them. Moreover, since the network needs an initial transient period to reach a realistic steady state (i.e., stationary buffer levels and link behaviors), we usually need a warm-up period (e.g., the first T_{wup} steps), during which no update is performed.

Following the approach of Solution 2, we perform a numerical analysis where the IAB-donor and IAB-nodes' DNNs are periodically updated assuming no transmission latency, K consecutive updates, and an initial warm-up period.

7 NUMERICAL RESULTS

In this section, we discuss the results of the performance tests of our MARL-based resource allocation approach on several instances considering IAB-nodes working in FD or HD mode, mobile UEs, and random link failures caused by mobile obstacles. Every value shown in the figures of this section is the result of an average over 10 random instances.

7.1 Scenario Settings

In line with 3GPP NR IAB simulation guidelines [1], we consider a $300\text{m} \times 300\text{m}$ service area where 1 IAB-donor is located at the left-side midpoint and 4 IAB-nodes are randomly deployed in the area. A set of 30 UEs move around in

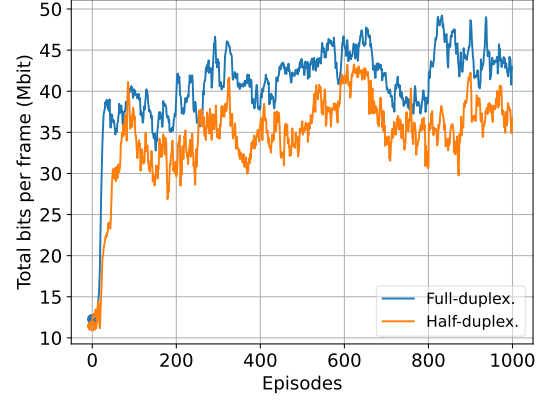


Fig. 6: Training curves in the FD and HD cases (UEs' speeds: 2m/s-20m/s, high density).

the area, with random initial positions and directions. The considered heights of IAB-donor, IAB-node and UE devices are 25m, 6m and 1.5m, respectively.

Both the IAB-donor and IAB-nodes are equipped with $N_p=4$ antenna panels, each of which manages $N_s=5$ sectors. The transmission power of each panel at the IAB-donor and at IAB-nodes is respectively 29.3 dBm and 20.3 dBm. The receiver noises at IAB-node and UE are -84.023 dBm and -82.023 dBm, respectively. The azimuth Half-Power BeamWidths (HPBW) for the IAB-donor and IAB-nodes are $\pi/36$ and $\pi/12$, and the elevation HPBW is $\pi/4$ for both. SINR thresholds and rates for MCSs in access and backhaul links are those indicated in MCS index table 3 for PDSCH in the 3GPP NR specification [42]. Finally, one frame consists of 80 slots, each with a duration $\delta=125\mu\text{s}$.

User mobility: UEs move in the playground according to a Random Waypoint model [36]. Specifically, a UE randomly selects a direction in the angular range $\xi \in [-180^\circ, 180^\circ]$ from the current direction. Then it travels along the selected direction with a constant speed uniformly chosen within the range $[2, 20]\text{m/s}$ ($[20, 60]\text{m/s}$ or $[60, 100]\text{m/s}$ in the extended analysis). Speeds and directions of different UEs are selected independently and randomly. After moving for $t_m \in [2, 6]\text{s}$, a UE pauses for an interval $t_p \in [0, 1]\text{s}$ before resuming. UEs bounce back when they reach the area boundary.

Obstacles: We assess the performance of our approach according to two levels of obstacle densities in the area and refer to them as *low* and *high*. They are implemented by dropping in the simulated service area, respectively, 15 and 60 cylindrical obstacles with a radius of 2.5m and a height of 2m. They move at a speed of 2m/s - 20m/s following the same Random Waypoint model applied to UEs.

7.2 MARL Model Settings

We train the DNN models of our approach for at most 5000 episodes, each of which consists of 80 steps (slots). This corresponds to a training period of 5000 frames, thus a total time of 50s. All DNN models have a hidden dimension of 128. We consider $K=4$ consecutive DNN updates, a data collection period for $T_{upd}=100$ steps, and a warm-up period of $T_{wup}=10$ episodes. The updates are performed via Adam

optimizer with a learning rate of 0.001 for both distributed policies and centralized critics. The weight ρ_{BH} for backhaul transmission in the reward function is set to 0.8. The discount factor γ is 0.99 and the weight τ of the policy network is set to 0.01. The weight vector $\bar{\psi}$ of target critic network, similarly to $\bar{\theta}$ of target actor network, is updated via $\bar{\psi} = \kappa\bar{\psi} + (1 - \kappa)\psi$ with update rate $\kappa = 0.001$. The replay buffer H has a maximum length of 10^6 entries, and each update uses mini-batches of 1024 entries, randomly sampled from H .

Training curves expressing the total traffic volume delivered in a frame from the IAB-donor to all the UEs (which corresponds to the throughput objective of the resource optimization problem) are shown in Fig. 6, where IAB-nodes operate in FD and HD modes, respectively. To better appreciate the learning behavior, we only show the first 1000 episodes, which involve the key performance-improving period before convergence. As we can see, the training process is immediately effective in increasing the throughput in both FD and HD. Indeed, blue and orange curves can reach high values just after less than 100 episodes, showing the model can learn fast from the experience. Nevertheless, we train it up to 5000 steps to let it accumulate sufficient experience and eventually obtain a stable performance in any situation.

7.3 Performance Analysis

In our previous work [22], we have shown how optimization-based resource allocation approaches cannot efficiently cope with the dynamics emerging in mmWave environments. Adaptive RL solutions typically lead to much better performance. However, to the best of our knowledge, all the RL-based scheduling approaches proposed so far for mmWave IAB networks do not consider mobile UEs, therefore they are inapplicable to the scenario we are considering. Therefore, we compare our approach based on MARL (MARL in the following) against the following three schemes:

- *MARL-NoIAB*: Our MARL-based approach where IAB-node relaying is disabled, forcing all UEs to connect directly to the IAB-donor.
- *RR*: A Round-Robin scheme where each panel of the IAB-donor and IAB-nodes iteratively serves slot-by-slot every UE under its coverage in a traditional round-robin fashion. If the number of bits in a queue of an IAB-node drops below a threshold, it will be refilled by its parent IAB-node in the next slot. This is a common scheduling scheme when dealing with wireless access transmissions.
- *RND*: A random scheme where each panel randomly picks an action from its candidate action set.

We begin the analysis for both FD and HD cases by considering typical UE urban speeds, in the range of 2m/s - 20m/s, to assess the impact of different obstacle densities on the performance, as shown in Figs. 7-9. Then, we extend our analysis to consider different speed ranges as reported in Fig. 10.

Traffic Volume and Data Rate: Figs. 7(a) and 8(a) show, respectively in the case of FD and HD, the average overall traffic volume delivered to UEs in one frame. Our MARL

scheme can achieve an improvement of 30% (FD) and 13% (HD) over the common RR scheme, as it can better coordinate interference among links and adapt its decisions to UEs' mobility, obstacle obstructions, and IAB-nodes' queue levels. The smaller gain in the HD mode is mainly due to the reduction of the degrees of freedom caused by duplex constraints at IAB-nodes. Indeed, the performance in the HD mode is strongly driven by backhaul transmissions to refill IAB-node buffers, which preclude access transmissions. Therefore, the overall result is less sensitive to the smart scheduling of access transmissions provided by MARL that is very effective in considering obstacles and mobility. In practice, these HD limitations prevent smart resource allocation schemes from fully exploiting all available wireless resources.

Another evident aspect is that MARL and RR schemes outperform MARL-NoIAB scheme, demonstrating that IAB nodes can remarkably boost the network throughput, even in simple tree-topologies as those recommended by 3GPP specifications. Note that MARL-NoIAB shows the same performance in FD and HD as it does not rely on IAB-nodes. Finally, compared to RR and RND schemes, MARL can better take advantage of the flexibility provided by FD operations, producing a larger improvement over HD than in the other approaches.

The number of bits downloaded by each UE in a frame produces the UE data rate. A comparison of the data rate averaged over the entire simulation achieved by the four schemes, under low and high obstacle densities, is reported in Figs. 9(a) and 9(b), respectively, in the cases of FD and HD. The lower and upper extremes of a bar respectively indicate the 25th percentile and 75th percentile of the distribution, the middle line is its median, and the green triangle indicates the mean value. As expected, higher obstacle densities lead to lower mean and top rates.

Given the direct relationship between frame traffic volume and data rate, we can observe the same general trends as the ones in Figs. 7(a) and 8(a). However, analyzing data rate figures we can further notice that the main advantage of MARL scheme over RR is due to a smarter exploitation of the UEs in good locations and channel conditions. Indeed, although showing similar median data rates, MARL allows to achieve a much better mean value than RR. This proves the ability of our approach to discover the most effective strategy to increase the overall throughput.

Coverage: Figs. 7(b) and 8(b) indicate the average percentage of served UEs per frame. We adopt two definitions of served UE: the first considers a UE served if experimenting an average data rate larger than 0Mbps, the second definition increases the minimum data rate to 50Mbps. Similarly to the above, the results for low and high obstacle densities are shown. The first aspect to note is that IAB-nodes have a strong impact on the coverage by remarkably enlarging the percentage of served UE, as we can see if we compare the results of MARL scheme with those of MARL-NoIAB scheme.

Some interesting aspects further emerge: considering the minimum data rate of 0Mbps, RR and RND schemes show higher percentages of served UEs than MARL scheme. This is a consequence of the throughput-vs.-fairness trade-off, while RR and RND schemes reach all UEs with the same

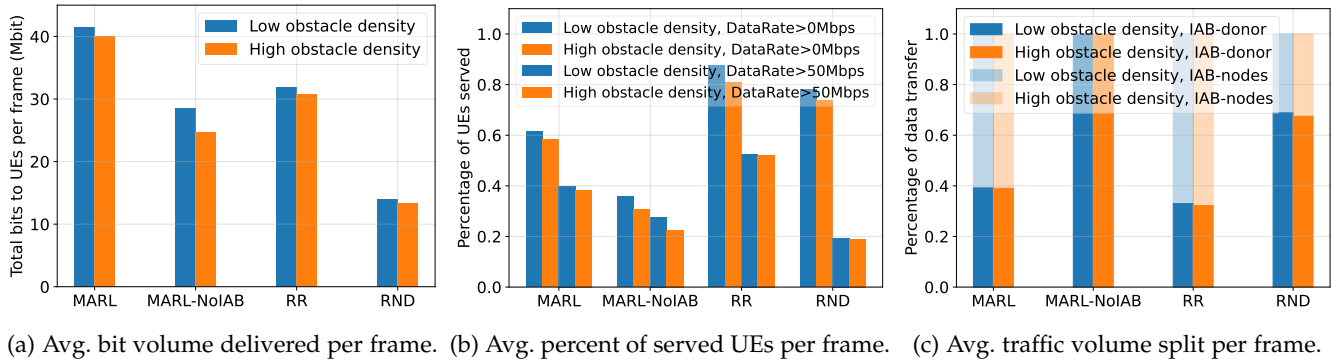


Fig. 7: Performance comparison of the four schemes in the FD case.

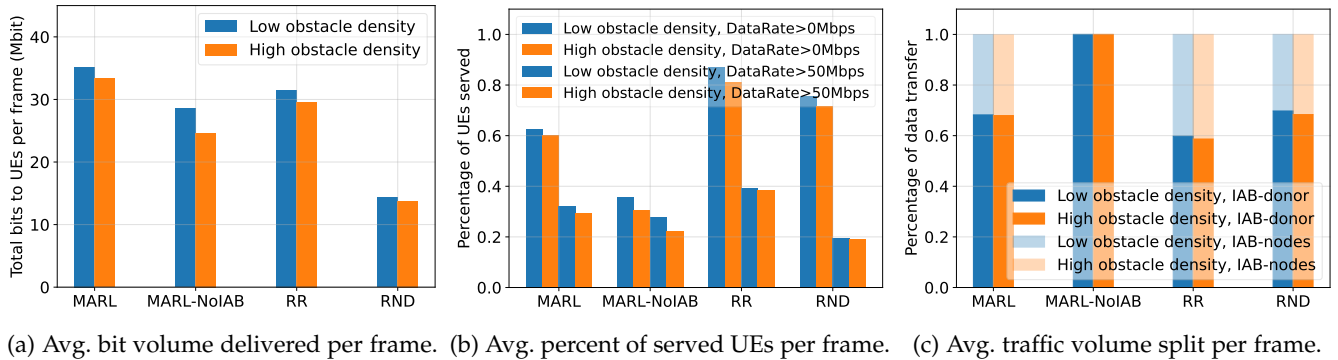


Fig. 8: Performance comparison of the four schemes in the HD case.

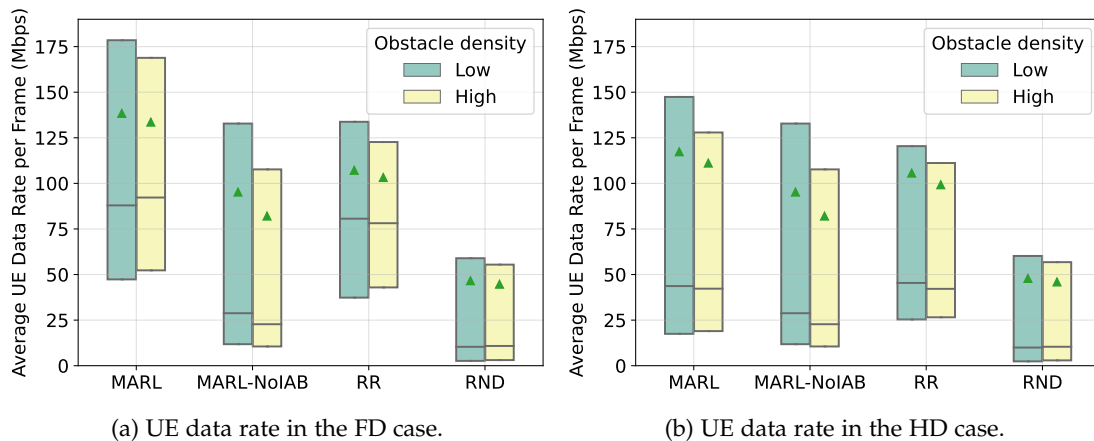


Fig. 9: Box plots of the average UE data rate per frame. Bottom, middle and top lines indicate respectively the 25th percentile, median, 75th percentile of the rate distribution. Green triangles indicate mean data rates.

probability, thus providing the best fairness, MARL scheme tends to preferably serve the UEs that provide the best overall throughput. However, we can also note that the difference remarkably reduces when considering UEs that experience at least 50Mbps. This confirms that the service guaranteed by RR and RND schemes is mainly driven by UEs with low data rates. This further demonstrates that the adaptive resource allocation of our MARL scheme can very effectively deal with intermittent links.

Backhaul Load: Figs. 7(c) and 8(c) provide an insight into the traffic volume delivered to UEs via the IAB wireless backhaul per frame. The upper translucent part of each

bar represents the average percentage of the traffic volume received by UEs from IAB-nodes via multi-hop, while the lower opaque part reports the complementary percentage of the traffic directly received from the IAB-donor. We can see that MARL scheme heavily resorts to backhaul IAB-nodes when operating in FD mode, even if the larger panels and the higher transmission power of the IAB-donor may lead UEs to directly connect to it. In the HD case, all the schemes reduce the load on the wireless backhaul. Indeed, HD IAB-nodes are less effective relaying nodes, causing transmission concurrency problems along the tree-like topology of the wireless backhaul.

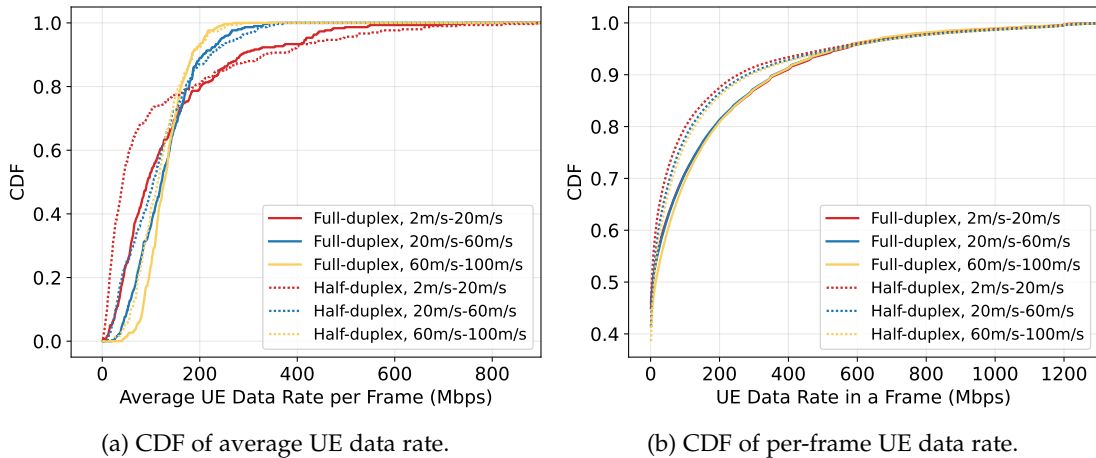


Fig. 10: CDFs of UE data rates achieved at different UE speeds and duplex modes.

UE Speed Sensitivity: Fig. 10 shows the performance of MARL scheme over different speed ranges in both FD and HD cases. Fig. 10(a) shows the cumulative distribution function (CDF) of the average data rate that a UE can experiment in a simulation. We can see that in both FD and HD cases, increasing speeds lead to a deterioration of the UE data rate. This was expected as fast moving UEs naturally create beam tracking issues. However, even at the extremely high speeds of $[20, 60]$ m/s, which can be rarely seen in the urban scenarios where such networks are envisioned, the impact on the performance is limited.

Fig. 10(b) shows the CDF of the data rate a UE achieves in a single frame. Despite different speed ranges, the curves considering the same duplex mode almost overlap. This implies that the effect of different UE speeds has in practice a negligible impact on the distribution of per-frame data rates across different UEs.

8 CONCLUSION

In this article, we have investigated the resource allocation problem in mmWave 5G IAB networks where user mobility and random obstructions caused by mobile obstacles produce strong network dynamics. Indeed, they generate short-lived access links and link-failure statistics that vary across different regions of the same service area. Leveraging these local network behaviors, we have proposed an MARL-based approach that splits a combinatorial monolithic SARRL problem, characterized by huge network state and action spaces, into smaller problems managed by different MARL agents located at IAB-nodes.

Through the cooperation among these MARL agents, we have developed a resource allocation framework that can coordinate link interference, monitor IAB-node buffer levels, and capture network dynamics. We have designed different MARL setups for full-duplex and half-duplex node operations. Moreover, we have provided a communication and coordination scheme for the training procedure that can solve potential feasibility issues (e.g., temporal dynamics) of real systems. The results of our numerical tests have shown that our MARL-based scheme can achieve good throughput performance without significantly harming the network fairness.

ACKNOWLEDGMENTS

This work was partially supported by China Scholarship Council (CSC) Grant No. 201806470077.

REFERENCES

- [1] 3GPP, *Study on integrated access and backhaul*, TR 38.874.
- [2] D. Yuan, H.-Y. Lin, J. Widmer, and M. Hollick, "Optimal joint routing and scheduling in millimeter-wave cellular networks," in *IEEE Conference on Computer Communications (INFOCOM)*, 2018, pp. 1205–1213.
- [3] A. Capone, I. Filippini, S. Gualandi, and D. Yuan, "Resource optimization in multi-radio multi-channel wireless mesh networks," in *Mobile Ad Hoc Networking: Cutting Edge Directions, Second Edition*, Wiley Online Library, 2013, pp. 239–274.
- [4] M. Polese, M. Giordani, A. Roy, D. Castor, and M. Zorzi, "Distributed path selection strategies for integrated access and backhaul at mmwaves," in *IEEE Global Communications Conference (GLOBECOM)*, 2018, pp. 1–7.
- [5] J. Kilpi, K. Seppänen, T. Suihko, J. Paananen, D. T. Chen, and P. Wainio, "Link scheduling for mmwave WMN backhaul," in *IEEE International Conference on Communications (ICC)*, IEEE, 2017, pp. 1–7.
- [6] M. Saad and S. Abdallah, "On millimeter wave 5G backhaul link scheduling," *IEEE Access*, vol. 7, pp. 76 448–76 457, 2019.
- [7] J. García-Rois, R. Banirazi, F. J. González-Castaño, B. Lorenzo, and J. C. Burguillo, "Delay-aware optimization framework for proportional flow delay differentiation in millimeter-wave backhaul cellular networks," *IEEE Transactions on Communications*, vol. 66, no. 5, pp. 2037–2051, 2018.
- [8] Y. Niu, W. Ding, H. Wu, Y. Li, X. Chen, B. Ai, and Z. Zhong, "Relay-assisted and QoS aware scheduling to overcome blockage in mmwave backhaul networks," *IEEE Transactions on Vehicular Technology*, vol. 68, no. 2, pp. 1733–1744, 2019.
- [9] Z. He, S. Mao, S. Kompella, and A. Swami, "Minimum time length scheduling under blockage and interference in multi-hop mmwave networks," in *IEEE Global Communications Conference (GLOBECOM)*, 2015, pp. 1–7.
- [10] Q. Hu and D. M. Blough, "Relay selection and scheduling for millimeter wave backhaul in urban environments," in *IEEE 14th International Conference on Mobile Ad Hoc and Sensor Systems (MASS)*, 2017, pp. 206–214.
- [11] C.-H. Yao, Y.-Y. Chen, B. P. Sahoo, and H.-Y. Wei, "Outage reduction with joint scheduling and power allocation in 5g mmwave cellular networks," in *2017 IEEE 28th Annual International Symposium on Personal, Indoor, and Mobile Radio Communications (PIMRC)*, IEEE, 2017, pp. 1–6.
- [12] H. Khan, A. Elgabri, S. Samarakoon, M. Bennis, and C. S. Hong, "Reinforcement learning-based vehicle-cell association algorithm for highly mobile millimeter wave communication," *IEEE Transactions on Cognitive Communications and Networking*, vol. 5, no. 4, pp. 1073–1085, 2019.

- [13] S. Khosravi, H. Shokri-Ghadikolaei, and M. Petrova, "Learning-based handover in mobile millimeter-wave networks," *IEEE Transactions on Cognitive Communications and Networking*, vol. 7, no. 2, pp. 663–674, 2020.
- [14] R. Kim, Y. Kim, N. Y. Yu, S.-J. Kim, and H. Lim, "Online learning-based downlink transmission coordination in ultra-dense millimeter wave heterogeneous networks," *IEEE Transactions on Wireless Communications*, vol. 18, no. 4, pp. 2200–2214, 2019.
- [15] F. Tang, Y. Zhou, and N. Kato, "Deep reinforcement learning for dynamic uplink/downlink resource allocation in high mobility 5G hetnet," *IEEE Journal on Selected Areas in Communications*, vol. 38, no. 12, pp. 2773–2782, 2020.
- [16] E. Pateromichelakis and K. Samdanis, "Context-aware joint routing & scheduling for mm-wave backhaul/access networks," in *IEEE Global Communications Conference (GLOBECOM)*, 2018, pp. 1–6.
- [17] N. Tafintsev, D. Moltchanov, M. Gerasimenko, M. Gapeyenko, J. Zhu, S.-p. Yeh, N. Himayat, S. Andreev, Y. Koucheryavy, and M. Valkama, "Aerial access and backhaul in mmwave b5g systems: Performance dynamics and optimization," *IEEE Communications Magazine*, vol. 58, no. 2, pp. 93–99, 2020.
- [18] L.-H. Shen and K.-T. Feng, "Mobility-aware subband and beam resource allocation schemes for millimeter wave wireless networks," *IEEE Transactions on Vehicular Technology*, vol. 69, no. 10, pp. 11 893–11 908, 2020.
- [19] W. Lei, Y. Ye, and M. Xiao, "Deep reinforcement learning based spectrum allocation in integrated access and backhaul networks," *IEEE Transactions on Cognitive Communications and Networking*, 2020.
- [20] T. K. Vu, C.-F. Liu, M. Bennis, M. Debbah, and M. Latva-Aho, "Path selection and rate allocation in self-backhauled mmwave networks," in *IEEE Wireless Communications and Networking Conference (WCNC)*, 2018, pp. 1–6.
- [21] T. K. Vu, M. Bennis, M. Debbah, M. Latva-Aho, and C. S. Hong, "Ultra-reliable communication in 5G mmwave networks: A risk-sensitive approach," *IEEE Communications Letters*, vol. 22, no. 4, pp. 708–711, 2018.
- [22] B. Zhang, F. Devoti, I. Filippini, and D. De Donno, "Resource allocation in mmwave 5g iab networks: A reinforcement learning approach based on column generation," *Computer Networks*, p. 108248, 2021.
- [23] M. Gupta, A. Rao, E. Visotsky, A. Ghosh, and J. G. Andrews, "Learning link schedules in self-backhauled millimeter wave cellular networks," *IEEE Transactions on Wireless Communications*, vol. 19, no. 12, pp. 8024–8038, 2020.
- [24] A. Ortiz, A. Asadi, G. H. Sim, D. Steinmetzer, and M. Hollick, "Scaros: A scalable and robust self-backhauling solution for highly dynamic millimeter-wave networks," *IEEE Journal on Selected Areas in Communications*, vol. 37, no. 12, pp. 2685–2698, 2019.
- [25] M. Feng and S. Mao, "Dealing with limited backhaul capacity in millimeter-wave systems: A deep reinforcement learning approach," *IEEE Communications Magazine*, vol. 57, no. 3, pp. 50–55, 2019.
- [26] M. Elsayed, M. Erol-Kantarci, and H. Yanikomeroglu, "Transfer reinforcement learning for 5g new radio mmwave networks," *IEEE Transactions on Wireless Communications*, vol. 20, no. 5, pp. 2838–2849, 2020.
- [27] T. Chu, J. Wang, L. Codecà, and Z. Li, "Multi-agent deep reinforcement learning for large-scale traffic signal control," *IEEE Transactions on Intelligent Transportation Systems*, vol. 21, no. 3, pp. 1086–1095, 2019.
- [28] D. Kwon and J. Kim, "Multi-agent deep reinforcement learning for cooperative connected vehicles," in *IEEE Global Communications Conference (GLOBECOM)*, 2019, pp. 1–6.
- [29] M. Sana, A. De Domenico, W. Yu, Y. Lostonlen, and E. C. Strinati, "Multi-agent reinforcement learning for adaptive user association in dynamic mmwave networks," *IEEE Transactions on Wireless Communications*, vol. 19, no. 10, pp. 6520–6534, 2020.
- [30] D. Guo, L. Tang, X. Zhang, and Y.-C. Liang, "Joint optimization of handover control and power allocation based on multi-agent deep reinforcement learning," *IEEE Transactions on Vehicular Technology*, vol. 69, no. 11, pp. 13 124–13 138, 2020.
- [31] B. Zhang and I. Filippini, "Mobility-aware resource allocation for mmwave iab networks via multi-agent rl," in *2021 IEEE 18th International Conference on Mobile Ad Hoc and Smart Systems (MASS)*, IEEE, 2021, pp. 17–26.
- [32] 3GPP, *Study on new radio access technology physical layer aspects*, TR 38.802.
- [33] Z. Xiao, P. Xia, and X.-G. Xia, "Full-duplex millimeter-wave communication," *IEEE Wireless Communications*, vol. 24, no. 6, pp. 136–143, 2017.
- [34] I. Filippini, V. Sciancalepore, F. Devoti, and A. Capone, "Fast cell discovery in mm-wave 5G networks with context information," *IEEE Transactions on Mobile Computing*, vol. 17, no. 7, pp. 1538–1552, 2017.
- [35] A. Maltsev *et al.*, "D5. 1-channel modeling and characterization," *MiWEBA Project (FP7-ICT-608637), Public Deliverable*, 2014.
- [36] F. Bai and A. Helmy, "A survey of mobility models," *Wireless Ad-hoc Networks. University of Southern California*, vol. 206, p. 147, 2004.
- [37] M. Gapeyenko, A. Samuylov, M. Gerasimenko, D. Moltchanov, S. Singh, M. R. Akdeniz, E. Aryafar, N. Himayat, S. Andreev, and Y. Koucheryavy, "On the temporal effects of mobile blockers in urban millimeter-wave cellular scenarios," *IEEE Transactions on Vehicular Technology*, vol. 66, no. 11, pp. 10 124–10 138, 2017.
- [38] M. Polese, M. Giordani, M. Mezzavilla, S. Rangan, and M. Zorzi, "Improved handover through dual connectivity in 5g mmwave mobile networks," *IEEE Journal on Selected Areas in Communications*, vol. 35, no. 9, pp. 2069–2084, 2017.
- [39] G. R. MacCartney, T. S. Rappaport, and S. Rangan, "Rapid fading due to human blockage in pedestrian crowds at 5G millimeter-wave frequencies," in *IEEE Global Communications Conference (GLOBECOM)*, 2017, pp. 1–7.
- [40] V. Mnih, A. P. Badia, M. Mirza, A. Graves, T. Lillicrap, T. Harley, D. Silver, and K. Kavukcuoglu, "Asynchronous methods for deep reinforcement learning," in *International Conference on Machine Learning (ICML)*, PMLR, 2016, pp. 1928–1937.
- [41] S. Iqbal and F. Sha, "Actor-attention-critic for multi-agent reinforcement learning," in *International Conference on Machine Learning*, PMLR, 2019, pp. 2961–2970.
- [42] 3GPP, *Physical layer procedures for data*, TS 38.214.



Bibo Zhang Bibo Zhang received the B.S. degree in information engineering and the M.S. degree in electronics and communication engineering from Beijing University of Posts and Telecommunications, China, in 2015 and 2018. She is currently pursuing the Ph.D. degree in information technology, from Politecnico di Milano, Italy. Her current research interests include resource management in 5G mmWave networks.



Ilario Filippini Ilario Filippini received B.S. and M.S. degrees in Telecommunication Engineering and a Ph.D in Information Engineering from the Politecnico di Milano, in 2003, 2005, and 2009, respectively. He is currently an Associate Professor with the Dipartimento di Elettronica, Informazione e Bioingegneria, Politecnico di Milano. His research interests include planning, optimization, and game theoretical approaches applied to wired and wireless networks, performance evaluation and resource management in wireless access networks, and traffic management in software defined networks. On these topics, he has published over 60 peer-reviewed articles. He serves in the TPC of major conferences in networking and as an Associate Editor of *IEEE Transactions on Mobile Computing and Elsevier Computer Networks*.